Jurnal Kejuruteraan 38(3) 2026: 1407-1417
https://doi.org/10.17576/jkukm-2026-38(3)-31

Photocatalytic Degradation of Methylene Blue Using ZrO_2/TiO_2-Chitosan Beads and Its Modelling by Artificial Neural Network (ANN)

Mohd Azam Mohd Adnan[a], Nurhidayatullaili Muhd Julkapli[b], Mohd Fadhil Majnis[c*], Mohd Arif Mat Norman[a], Zahirrudin Idris[a] & Saba Afzal[d]

[a]*Advanced Materials & Manufacturing Research Group (AMMRG), Faculty of Engineering and Life Sciences, University of Selangor, 45600 Bestari Jaya, Selangor, Malaysia*

[b]*Nanotechnology and Catalysis Research Center (NANOCAT), Level 3, Block A, Institute for Advanced Studies (IAS), Universiti Malaya, 50603 Kuala Lumpur, Malaysia*

[c]*Faculty of Chemical Engineering, Universiti Teknologi MARA, 40450 Shah Alam, Selangor, Malaysia.*

[d]*Department of Chemistry, Sardar Bahadur Khan Women's University, Quetta 87300, Pakistan*

[*]*Corresponding author: fadhilmajnis@uitm.edu.my*

Received 12 August 2025, Received in revised form 7 February 2026
Accepted 7 March 2026, Available online 30 May 2026

ABSTRACT

The epidemic growth of the textile industries over the years to meet human demands has exerted substantial pressure on the global environment, particularly in the synthetic dyes waste crisis. Herein, the photocatalytic degradation of methylene blue (MB) synthetic dye was investigated using a ternary system of ZrO_2, TiO_2 and chitosan in bead forms. The investigation parameters involved composition ratio, concentration of ppm and catalyst doses. The experimental data demonstrated that ZrO_2 /TiO_2 /CS achieved a remarkable MB removal rate of 94.3% at a ratio of 1:1:1. This photocatalytic system effectively removed the dye from the solution. Additionally, using 3 g of the photocatalyst, the adsorption process resulted in 94.8 % completion. Notably, the photocatalyst achieved efficient colour removal at a concentration of 5 ppm. The Artificial Neural Network (ANN) modelling also revealed that the predicated model perfectly fitted with the experimental data. This research provides valuable perspectives on utilizing ZrO_2/TiO_2-Chitosan beads for photocatalytic degradation and illustrates the efficacy of ANN modelling in forecasting photocatalytic efficiency.

Keywords: Ternary system; photocatalytic degradation; artificial neural network; methylene blue; degradation mechanism

INTRODUCTION

Water is a vital resource for all life on earth and is considered one of the most valuable assets for human civilization. Ensuring access to clean, safe, and affordable water is one of the most pressing global challenges of the 21st century. The contamination of water bodies with industrial dyes poses significant environmental pollution and human health risks (Manoharan et al. 2023; Saad et al. 2023). Traditional physicochemical treatment methods have efficiency and environmental impact limitations, such as membrane filtration, coagulation-flocculation, flotation, precipitation, ion exchange, adsorption, ultrasonic mineralization, ion-pair extraction, and electrolysis (Jallouli et al. 2022; Ammar et al. 2023; Kerkulah et al. 2023).

Photocatalytic degradation has emerged as a promising solution for removing pollutants from water due to its non-toxic, cost-effective, and efficient nature (Kumari et al. 2023; Taib et al. 2023). Recent advancements in titanium dioxide (TiO_2) based nanomaterials have demonstrated their high photocatalytic activity under UV light irradiation, effectively degrading various pollutants without causing

secondary pollution (Madkhali et al. 2023; 9. El Sharkawy et al. 2023). Integrating chitosan with the semiconductor system is anticipated to enhance the photocatalytic efficiency of TiO_2, thereby improving the removal of dye pollutants from wastewater (Majnis et al. 2022; Adnan et al. 2022a; Kasinathan et al. 2023).

Artificial Neural Networks (ANNs) have been increasingly employed to model and optimize environmental processes, including pollutant degradation and remediation. Several studies have shown that ANNs can accurately predict process behaviours and replicate experimental data, making them valuable tools for optimizing photocatalytic systems (Akerdi et al. 2020; Rezai & Allahkarami, 2021). Recent research has demonstrated the application of ANNs in various environmental processes, such as predicting the degradation efficiency of different pollutants under varying conditions (Luo et al. 2023) and optimizing the operational parameters for maximum efficiency (Jana et al. 2022). For instance, The ANN model can accurately estimate the removal efficiency of biological oxygen demand, total nitrogen, total phosphorus, and total suspended solids in wastewater treatment plants with an R-value of 0.9909 and a mean squared error (MSE) of 5.962 (Alnajjar & Üçüncü, 2023).

Despite these progressions, creating a photocatalyst that effectively breaks down dye pollutants at different concentrations poses difficulties. The research objective was to tackle this issue by producing and examining a three-component hybrid photocatalyst comprised of ZrO_2, TiO_2, and chitosan while assessing its ability to degrade methylene blue. In addition, the implementation of ANN in this study was to predict the degradation effectiveness under various circumstances, offering valuable perspectives for improving the photocatalytic process.

METHODOLOGY

SYNTHESIS OF THE CATALYST

A 2% acetic acid solution was prepared by combining 500 mL of deionized water with 10 mL of acetic acid. Chitosan was then dissolved in the acetic acid solution, and the resulting mixture was agitated for 1 hour to ensure homogeneous dispersion of the chitosan. Subsequently, dissolved titanium dioxide (TiO_2) was added to the suspension, which was stirred for an additional hour to achieve uniform distribution of the TiO_2. Finally, zirconium dioxide (ZrO_2) was introduced to the TiO_2 suspension, and the mixture was agitated for a further hour to guarantee uniform incorporation of the zirconium. The solution was then continuously stirred for 24 hours.

CHARACTERIZATION

Field Emission Scanning Electron Microscopy (FESEM) was employed to analyze the surface characteristics of the samples. The FEI Quanta 450 FEG was used to examine the composite's surface morphology. To investigate functional groups and chemical linkages between ZrO_2, TiO_2, and Chitosan, Fourier Transform Infrared spectroscopy with a PerkinElmer 100 spectrophotometer was carried out. Prior to sample placement, the sample holder was cleaned with acetone. A mixture of a small amount of ZrO_2/TiO_2/Chitosan sample (0.3 mg) and 4 mg of KBr was formed into a pellet before being placed on the sample holder for IR spectral analysis within the range of 400 – 4000 cm^{-1} to assess molecular vibrational energies.

PHOTOCATALYTIC ACTIVITIES

The photocatalytic activity of the synthetic ratio 1:1:1, 2:1:1, and 3:1:1 was investigated, considering the degradation percentages of MB dye under a visible light source. The photocatalytic system, composed of a visible light source incorporated in the study, was a metal halide lamp (250 W). The average intensity of the incident light and the average length were measured. All the photocatalytic tests were performed after achieving the adsorption/desorption equilibrium and after considering the removal values from the predicted photolysis reactions. The selected factors in the study included the composition ratio, MB concentrations(ppm), catalyst doses and the reusability cycles of the used photocatalyst. The MB degradation percentages were estimated based on the detection of the residual dye concentrations after each UV–vis spectrophotometer test. The degradation (%) of MB was calculated according to Equation (1).

$$\%\ Photodegradation = \frac{(C_o - C)}{C_o} \times 100\% \quad (1)$$

where
C_o is the initial concentration of MB,
C is the concentration after photo-irradiation.

The photodegradation of MB obeys the pseudo-first-order kinetics according to the Langmuir–Hinshelwood

model. The following Equation (2) was interpreted as the photodegradation rate of MB, λmax of 664 nm.

$$ln\frac{C}{C_o} = -kt \quad (2)$$

where
C/C_o is the normalized MB concentration at time t, k is the apparent rate constant, min^{-1}.

ARTIFICIAL NEURAL NETWORK (ANN) MODELLING PROCEDURE

The Artificial Neural Network approach has emerged as a prominent tool for predicting output based on input parameters. ANN can be characterized as a mathematical analogue of the human brain, capable of recognizing intricate patterns. Training the ANN model requires providing it with input data and the corresponding target output. This study utilized approximately 150 input data sets to train the ANN model, further divided into training, validation, and testing subsets.

FORMULATION OF INPUT DATA FOR TRAINING ARTIFICIAL NEURAL NETWORK MODELS

Effective ANN model development necessitates training the model with pertinent input data and corresponding target outputs to enable accurate predictions. In the present study, the input data encompassed various parameters associated with the photocatalytic degradation of methylene blue using a TiO_2/ZrO/CS composite material. These parameters included the initial MB concentration, the dosage of the composite material, and the irradiation duration of the process. The target output for the ANN model was the percentage of methylene blue degradation achieved under the specified conditions.

The minimum number of training samples required for the ANN model was established using a specific Equation (3), which served as a guideline for the model (Norman et al. 2022). This approach accounted for the number of nodes in the hidden, input, and output layers to determine the necessary training data set size. Concurrently, the quantity of hidden layer nodes was determined using Equation (4) (Sheela & Deepa, 2013).

$$T_n = h_n\,(i_n + 1) + O_n(h_n + 1) \quad (3)$$

$$h_n = \frac{3i_n}{i_n - 1} \quad (4)$$

Where;
T_n is the minimum number of training data sets,
h_n is the number of hidden layer nodes,
i_n is the number of input layer nodes,
O_n is the number of nodes in output layers.

RESULTS

SURFACE MORPHOLOGY OF HYBRID CATALYST

The distribution and surface structure of ZrO_2/TiO_2 nanoparticles within the chitosan (CS) matrix were analyzed using field emission scanning electron microscopy (FESEM). All photocatalysts exhibited a macro-reticular structure with spherical or irregularly spherical primary CS and ZrO_2/TiO_2 nanoparticles. Figure 1 presents images of the hybrid photocatalyst with different component ratios: (a) 1:1:1, (b) 2:1:1, and (c) 3:1:1, confirming the linkage between synthesized ZrO_2/TiO_2 and CS. The 1:1:1 sample showed tightly packed, spherical nanoparticles, indicating a high level of synthesis control. The rough, granular surface texture suggested a substantial surface area, advantageous for applications requiring extensive surface interactions. The uniform particle distribution with minimal agglomeration pointed to a homogeneous blend of ZrO_2, TiO_2, and CS, further confirming the precision of the synthesis process. The 2:1:1 sample exhibited a more heterogeneous texture, characterized by a mix of more extensive, irregular particles and smaller ones. This textural diversity resulted from larger agglomerates within the sample. While the overall distribution appeared uniform, some regions showed denser clustering, suggesting partial agglomeration due to a higher concentration of one component. The 3:1:1 sample displayed significantly more prominent and irregularly shaped particles, leading to a highly heterogeneous texture. This suggested a complex internal structure with notable particle size and surface roughness disparities. The particle distribution was less uniform, with visible clusters and agglomerates, potentially due to the increased proportion of one constituent, impacting overall homogeneity. These morphological features were expected to enhance photocatalytic activity by improving interactions with incident light photons during the photocatalytic degradation of organic pollutants.

CHEMICAL ANALYSIS OF HYBRID CATALYST

\The active surfaces and functional groups of the prepared photocatalysts can be determined by Fourier Transform Infrared (FTIR) spectroscopy analysis.

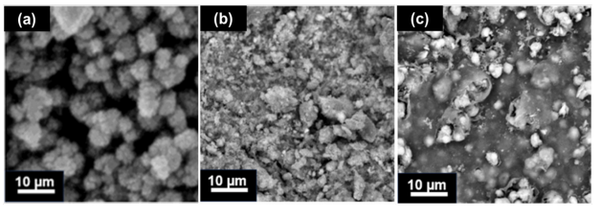

FIGURE 1. FESEM images samples of as-formed ZrO_2/TiO_2/CS nanocomposite with different ratios of (a) 1:1:1, (b) 2:1:1 and (c) 3:1:1.

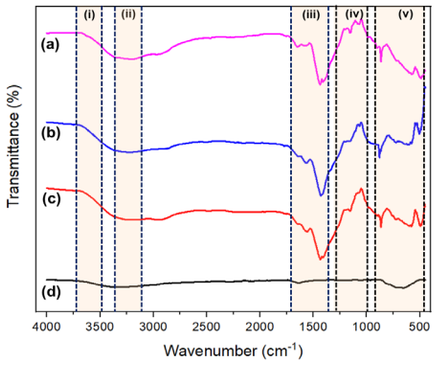

FIGURE 2. FT-IR spectrum of ternary with different ratios of ZrO_2/TiO_2/CS nanocomposites (a) 3:1:1, (b) 2:1:1, (c) 1:1:1 and (d) pure TiO_2

This analytical technique was utilized to investigate the binding properties of the functional groups within the as-prepared ZrO_2/TiO_2/chitosan nanocomposite materials. The FTIR spectra of ZrO_2/TiO_2/CS nanocomposites with varying compositional ratios have been presented in Figure 2, covering the wavenumber range from 4000 cm^{-1} to 400 cm^{-1}. This spectral information provided insights into the chemical bonding and functional groups present in the samples, which included (a) ZrO_2/TiO_2/CS in a 3:1:1 ratio, (b) ZrO_2/TiO_2/CS in a 2:1:1 ratio, (c) ZrO_2/TiO_2/CS in a 1:1:1 ratio, and (d) pure TiO-. The corresponding FTIR peak assignments have been tabulated in Table 1.

The prominent absorption bands observed in the 3477-3724 cm^{-1} spectral region can be attributed to the interaction between O-H bonds, particularly those involving hydroxyl and amine groups (Huang, & Peng, 2021). This indicated the presence of hydroxyl groups and hydrogen bonding interactions within the composite materials. The 3100-3345 cm^{-1} region exhibited characteristic stretching vibrations of O-H and N-H functional groups, suggesting a significant presence of hydroxyl and amine functionalities in the composite matrix (Tian et al. 2019). The spectral region between 1310-1680 cm^{-1} exhibited absorption features characteristic of the stretching vibrations of hydroxyl, primary amine, and ether functional groups, indicating the presence of amines within the composite material. Furthermore, the 970-1270 cm^{-1} region displayed stretching vibrations associated with C-N, C-H, and C=C functionalities, suggesting the incorporation of organic components containing nitrogen and unsaturated carbon moieties (Wu et al. 2023). Furthermore, this spectral region 450-950 cm^{-1} exhibited C-H stretching vibrations associated with the C-O group in amide II stretching modes and absorption bands corresponding to Ti-O, Zr-O, and Ti-O-Ti bonds (Tian et al. 2019). These features confirmed the incorporation of titanium dioxide and zirconium dioxide nanoparticles within the composite materials.

TABLE 1. FT-IR peaks of ternary system ZrO_2/TiO_2/CS composites

Symbol/ Region	Position band/ Wavenumber (cm^{-1})	Possible Assignment
i	3477-3724	–OH bonds interaction between HO-NH
ii	3100-3345	OH–NH functional group
iii	1310- 1680	Stretching vibration of –OH and –NH2 Signal of C-N and C-H bending vibration C=C group vibration
iv	970-1270	–CH stretching vibration associated with C–O group amide II (–NH bending vibration in NH_2) Symmetric deformation band CH_3
v	450-950	TiO-band, O–TiO–O stretching band

The 3:1:1 ratio sample (a) displayed pronounced spectral features across all identified regions, indicating robust interactions among the ZrO_2, TiO_2, and CS components. The high peak intensities observed in regions I and II suggested the presence of significant hydrogen bonding and functional group interactions. The 2:1:1 ratio sample (b) displayed comparable spectral features but with marginally lower peak intensities, signifying a proportional decline in the extent of specific interactions and functional group prevalence. The 1:1:1 ratio sample (c) exhibited

attenuated peak intensities, particularly in regions I and II, indicating a diminished concentration of OH and NH_2 functional groups due to the equimolar composition. Conversely, the pure TiO_2 sample (d) displayed prominent peaks primarily in region V, corresponding to Ti-O and Ti-O-Ti bonds, with minimal contributions from organic functional groups (Adnan et al. 2022a).

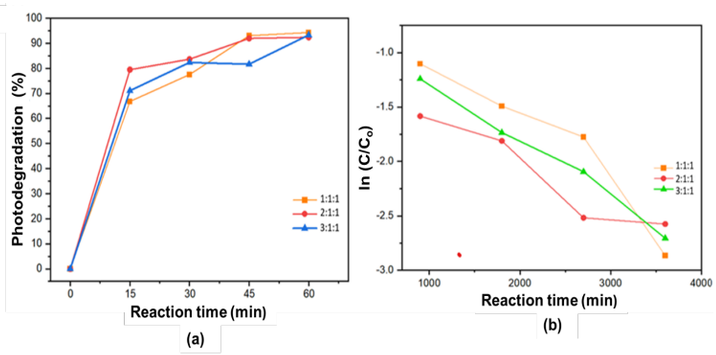

FIGURE 3. (a) Photodegradation efficiency of samples with a variant composition ratio towards MB (b) rate of reaction

PHOTODEGRADATION OF MB UNDER VISIBLE LIGHT IRRADIATION

EFFECT OF PHOTOCATALYSTS COMPOSITIONRATIO

The photocatalytic efficiency of the hybrid ZrO_2/TiO_2/CS catalyst was evaluated by studying the photochemical breakdown of methylene blue. The solutions were stirred in darkness for 60 minutes prior to irradiation to ensure a balance between adsorption and desorption of the pollutant on the photocatalyst. Three different proportions of the ZrO_2/TiO_2/CS catalyst (1:1:1, 2:1:1, and 3:1:1) were examined for their ability to degrade MB (Figure 3). Samples were collected at intervals of every 15 minutes throughout the irradiation process. Each catalyst composition was evaluated using a ten ppm MB solution at pH 7 with 1 g of the catalyst. The results revealed that Sample 1 (1:1:1) demonstrated the highest percentage of MB decolorization at 94.3%, followed by Sample 3 (3:1:1) at 93.3% and Sample 2 (2:1:1) at 92.4%. Furthermore, Sample 1 exhibited the highest reaction rate of 2.86 min^{-1}, indicating its excellent photocatalytic activity compared to the other samples. In contrast, Sample 2 displayed the lowest reaction rate at 2.57 min^{-1} while showing less stable decolourization over time compared to Sample 1 despite having a slightly similar decolourization percentage. Sample 1 (1:1:1) was selected for further investigation based on its excellent degradation percentage and stable decomposition rate.

EFFECT OF CATALYST DOSAGES

The adsorption and photocatalytic activity of the ZrO_2/TiO_2/CS nanocomposite photocatalyst was investigated with different catalyst dosages of 1 g, 2 g, 3 g, 4 g, and 5 g. Sample 1 (1:1:1) was applied to MB at a concentration of 10 ppm (pH 7) for this experiment. Figure 4 shows the Effect of the catalyst dosage for MB on the percentage efficiency of colour removal and the reaction rate of the process.

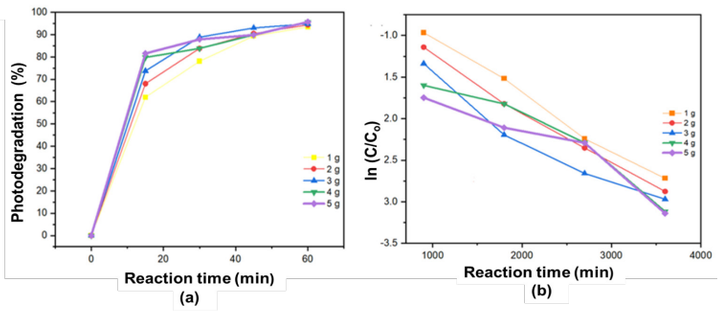

FIGURE 4. (a) Photodegradation efficiency of samples with a variant composition ratio towards MB (b) rate of reaction

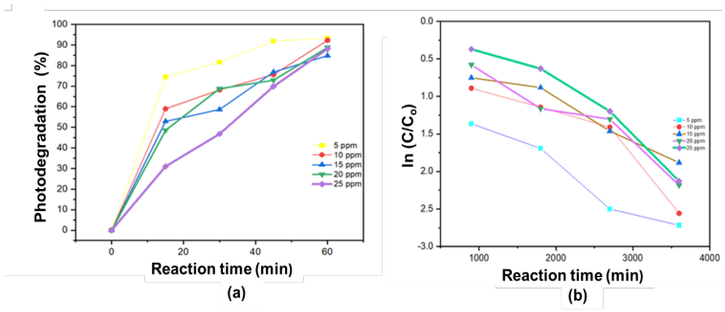

FIGURE 5. (a) Photodegradation percentage of samples with a variant concentration of MB (b) rate of reaction

The inclusion of ZrO_2 improved the photochemical breakdown of MB. ZrO_2 is recognized for its potent photocatalytic capability in breaking down organic contaminants (Hassan & Jalil, 2022). The decomposition rate rose with the amount of catalyst up to a certain level, yielding the best results and exceeding this optimal amount, which led to reduced fading of the wastewater. The most effective dosage was determined to be 3 g. For a 3 g catalyst, the adsorption process achieved 94.80% methylene blue (MB) degradation after 1 hour of exposure, with a reaction rate of 2.96 min^{-1}. In comparison, the degradation percentages for catalyst dosages of 1 g, 2 g, 4 g, and 5 g were 93.4%, 94.4%, 95.6%, and 95.67%, respectively, with corresponding reaction rates of 2.71, 2.87, 3.11, and 3.13 min^{-1}. The variances were ascribed to the variation in the number of active sites accessible in the procedure. This resulted in an augmented generation of hydroxyl radicals and superoxides, thereby boosting the decomposition process (Wang et al. 2022). Nevertheless, surpassing the optimum value for catalyst dosage can diminish degradation effectiveness. This decrease is triggered by heightened suspension turbidity and diminished light penetration due to increased light scattering impacts (de Moraes et al. 2018). Therefore, an optimal catalyst dosage of 3 grams was determined to achieve high degradation efficiency with a well-balanced reaction rate and minimal light scattering, thus warranting its suitability for subsequent experiments.

EFFECT OF CONCENTRATION

The adsorption and photochemical degradation of methylene blue (MB) was further investigated at different concentrations (5 ppm, 10 ppm, 15 ppm, 20 ppm, and 25 ppm) using sample 1 (3 g of catalyst). The influence of ZrO_2 loading on the percentage degradation of MB was evaluated at these concentrations. Figure 5 depicts the impact of dye concentration on MB degradation, demonstrating (a) the proportion of decolourization and (b) the reaction rate of the process. The slowest complete degradation was observed with the 10 ppm dye solution, followed by the 15 ppm, 20 ppm, and 25 ppm solutions. In contrast, the 5 ppm dye solution completely degraded within merely 30 minutes. This suggested that initial concentration exerts a substantial influence on the degradation rate. As the initial concentrations of dye increase, the dye molecules attach to the surface of the catalyst, and a considerable amount of light radiation is absorbed by the dye molecules rather than the ZrO_2/TiO_2 particles. The adsorption rate was at its highest at 93.4% for 5 ppm. The efficiencies for removing dyes in solutions with concentrations of 10 ppm, 15 ppm, 20 ppm, and 25 ppm were found to be 92.3%, 84.8%, 88.7%, and 88.1% respectively. The most effective removal percentage was achieved with a concentration of 5 ppm where higher concentrations lead to a slower formation of hydroxyl radicals (OH*) due to fewer photons reaching the photocatalyst's surface (Din & Khalid, 2023).

REUSABILITY STUDY

The investigation focused on the potential for reusing the ZrO_2/TiO_2/CS nanocomposite photocatalyst in multiple MB dye degradation cycles, as shown in Figure 6.

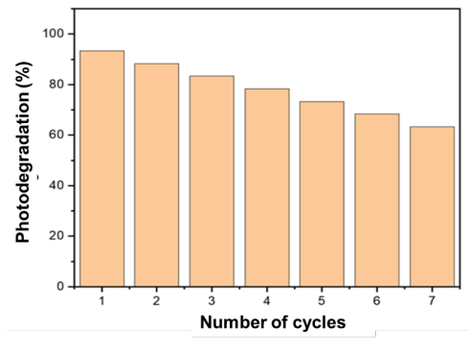

FIGURE 6. Reusability test for the photocatalytic studies a degradation efficiency during seven cycles

Heterogeneously catalyzed reactions offer the beneficial feature of catalyst reusability. The photodegradation efficiency of the fresh ZrO_2/TiO_2/CS catalyst showed a slight decrease after each cycle, with colour removal percentages decreasing from 93.4% in the first cycle to 63.4% in the seventh cycle. The slight reduction in photocatalytic effectiveness during repeated cycles may result from the accumulation of intermediate substances that could have impacted the catalytic sites (Bagheri et al. 2017). Nevertheless, due to its improved properties, the ZrO_2/TiO_2/CS compound catalyst displayed enhanced initial photocatalytic performance. However, as impurities adhered to the photocatalyst over time, there was a marginal deterioration in its structural characteristics, leading to a decrease in efficiency from the first cycle to the seventh (Adnan et al. 2022a; Adnan et al. 2022b).

ANN MODEL DEVELOPMENT

Three-layer Artificial Neural Network models (ANN) were developed and trained using the backpropagation gradient descent algorithm in MATLAB R2014a (MathWorks Inc.). The transfer function applied to both the input and hidden layers was the hyperbolic tangent sigmoid function (tansig), while a linear function was used for the output layer. One hundred experimental data points were randomly divided into training, validation, and test sets. During training, the Levenberg-Marquardt (LM) algorithm was used to update the weights and bias of the ANN models, using the training set for this purpose. The generalizability of the model was assessed using the test set. The error of the validation set was monitored during training to avoid overfitting. Using the RE datasets obtained from the experiments, ANN models were developed to determine the effects of the operational parameters on degrading the MB. The selected training function and number of hidden neurons have been detailed in Table 2. Furthermore, Figure 7 illustrates the chosen ANN architecture, which comprises 3 input layers, 1 output layer, and 1 hidden layer with a specified number of neurons. This specific network configuration was identified as the optimal design after evaluating various training algorithms.

Artificial Neural Networks (ANN) were effectively used to forecast the decline in MB percentage throughout the experiment. Through experimentation, the ideal number of neurons in the hidden layer was determined to minimize mean squared error during training (Shahryari et al. 2013). The Levenberg-Marquardt algorithm was selected for its ability to achieve low MSE. The ANN models were developed using MATLAB 2022b software.

TABLE 2. Selected training function and hidden neuron

Parameters	Value
Input Neurons	03 (concentration, time, dose)
Output Neurons	01 (degradation)
Number of Hidden Layers	5
Transfer function	TANSIG (tangent sigmoid)
Learning cycle	50 epochs
Performance function	MSE (Mean Squared Error)
Data division function	Random
Data division	70%-15%-15%
Training function	Levenberg Marquardt (LM)

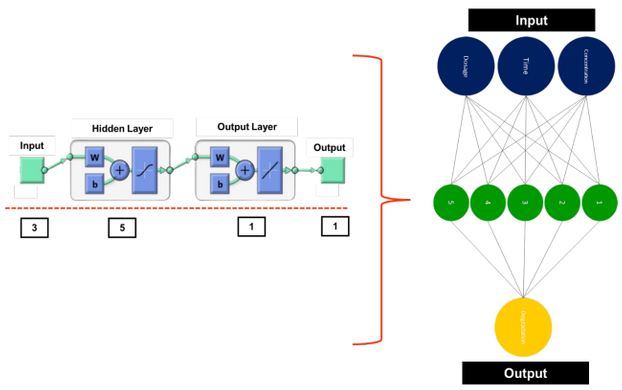

FIGURE 7. ANN network architecture

TABLE 3. Prediction of the experimental results of MB degradation (%)

No	Concentration (ppm)	Time(min)	dosage (g)	MB degradation (%)	Predicted (%)	%Error (%)
1	5	15	3	74.44	69.13	7.13
2	5	30	3	81.61	77.94	4.5
3	5	45	3	91.8	92.61	0.88
4	5	60	3	93.4	105.1	12.52
5	10	15	3	59.1	58.95	0.25
6	10	30	3	68.14	67.47	1.46
7	10	45	3	75.6	83.68	10.69
8	10	60	3	92.3	95.25	3.2
9	15	15	3	52.9	43.24	18.26
10	15	30	3	58.7	61.51	4.79
11	15	45	3	76.84	76.86	0.03
12	15	60	3	84.78	83.16	1.91
13	20	15	3	48.6	43.46	10.58
14	20	30	3	68.76	62.89	8.54
15	20	45	3	72.87	76.28	4.68
16	20	60	3	88.74	78.89	11.1
17	25	15	3	31.02	43.9	41.52
18	25	30	3	46.78	45.43	2.89
19	25	45	3	69.84	67.9	2.78
20	25	60	3	88.11	87.33	0.9

The network consisted of three input neurons representing time in minutes, dose in grams, and concentration in ppm and one output neuron for the MB degradation percentage. The dataset from 20 trials was divided into training (70%), validation (15%), and testing (15%) sets, which have been tabulated in Table 3. Figure 8 illustrates the anticipated and observed degradation percentage for ZrO_2/TiO_2/CS.

The regression analysis conducted on the training data for the selected artificial neural network models demonstrated a robust correlation between the predicted and observed degradation percentages of MB by the TiO_2/ZrO/CS composite material (Figure 8 (b)). The comprehensive regression plot exhibited a high coefficient of determination, indicating the solid predictive performance of the ANN model, with most predicted values closely aligning with the actual observations. Additionally, the regression line's slope of approximately 0.97501, close to the ideal value of 1, suggested that the ANN model achieved near-perfect predictive accuracy. The model demonstrated solid predictive capabilities on the validation data, as evidenced by a high correlation coefficient of 0.97959. This suggested that the model could generate accurate prediction results for new test input data. While the regression line exhibited a slight deviation from the ideal, this could be attributed to the relatively limited size of the validation set. Additionally, the model's performance on the test data set yielded an almost perfect correlation coefficient (R= 0.99999). This exceptional R-value demonstrated that the model predicted MB degradation with high accuracy on the test data, confirming the robustness and reliability of the ANN model. The regression equation suggested a slight overestimation, similar to the training data set. The ANN model showed strong predictive performance with high correlation coefficients across training, validation, and test datasets. The slight deviations in regression equations indicated minor biases that could be further optimized. Overall, the ANN model was highly effective in predicting the photocatalytic degradation of MB using TiO_2/ZrO/CS composite material, demonstrating its utility in guiding experimental and practical applications.

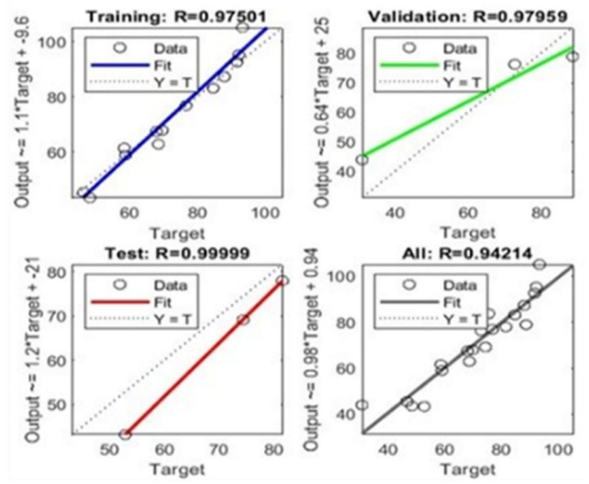

FIGURE 8. Regression plot ANN model rends in training, validation, test, and all

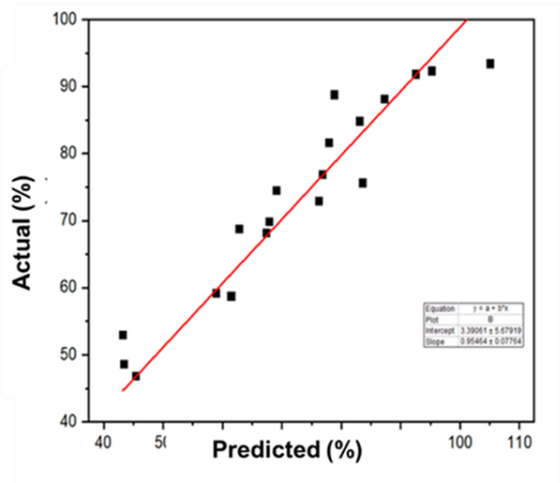

FIGURE 9. Predicated vs actual degradation percentages for MB

Figure 9 presents a comparative visualization of the predicted and experimentally determined degradation percentages for methylene blue. The proximity of the data points to the ideal reference line indicated a strong agreement between the forecasted and observed values. The reported linear equation y = 0.9564x + 5.6799 and the associated coefficient of determination (R^2) suggested a robust linear relationship, though the slope being less than unity implied that the model tended to underestimate the actual degradation levels slightly. The Artificial Neural Network model demonstrated precise predictions during training and testing. High R^2 values indicated a close match between the predicted percentage degradation by ANN and the actual patterns observed (Apaydin et al. 2021; Zulfiqar et al. 2019).

CONCLUSION

The study revealed that a ternary catalyst bead composed of ZrO_2/TiO_2/CS exhibited outstanding photocatalytic characteristics. FTIR analysis verified the uniform distribution of ZrO_2/TiO_2 within the CS matrix and identified significant functional groups such as M=O bonds and carbonate anions. Sample 1 (1:1:1) demonstrated the most effective adsorption and photocatalytic performance among the samples tested, with a degradation rate of 94.3% attributed to the favourable ZrO_2/TiO_2/CS ratio. The efficiency of photocatalysis declined as pollutant concentrations increased, leading to reduced photon absorption at surface saturation. An artificial neural network model utilizing concentration, time, and dosage as input parameters successfully forecasted degradation rates with a high degree of correlation to experimental findings. Overall, this research provides valuable perspectives on utilizing ZrO_2/TiO_2/CS bead for photocatalytic degradation and illustrates the efficacy of ANN modelling in forecasting photocatalytic efficiency.

ACKNOWLEDGEMENT

The authors acknowledge the Ministry of Higher Education, Malaysia, for the financial support through the Fundamental Research Grant Scheme (FRGS) funding. Project code: FRGS/1/2022/TK09/UM/02/28

DECLARATION OF COMPETING INTEREST

None.

REFERENCES

Adnan, M. A. M., Afzal, S., Johan, M. R., & Julkapli, N. M. 2022a. A comparative study on the photodegradation efficiency of TiO_2-CS hybrid beads under wet and dry conditions. *International Journal of Materials and Product Technology* 65(1): 67-79.

Adnan, M. A. M., Phoon, B. L., Johan, M. R., Tajaruddin, H. A., & Julkapli, N. M. 2022b. Visible light-enable oxidation and antibacterial of zinc oxide hybrid chitosan photocatalyst towards aromatic compounds treatment. *Materials Today Communications* 32: 103956.

Akerdi, A. G., Bahrami, S. H., & Pajootan, E. 2020. Modeling and optimization of Photocatalytic Decolorization of binary dye solution using graphite electrode modified with Graphene oxide and TiO_2. *Journal of Environmental Health Science and Engineering* 18: 51-62.

Alnajjar, H. Y., & Üçüncü, O. 2023. Removal efficiency prediction model based on the artificial neural network for pollution prevention in wastewater treatment plants. *Arab Gulf Journal of Scientific Research* 41(4): 610-626.

Ammar, M., Yousef, E., Mahmoud, M. A., Ashraf, S., & Baltrusaitis, J. 2023. A Comprehensive Review of the Developments in Electrocoagulation for the Removal of Contaminants from Wastewater. *Separations* 10(6): 337.

Apaydin, H., Sattari, M. T., Falsafian, K., & Prasad, R. (2021). Artificial intelligence modelling integrated with Singular Spectral analysis and Seasonal-Trend decomposition using Loess approaches for streamflow predictions. *Journal of Hydrology* 600: 126506.

Bagheri, S., TermehYousefi, A., & Do, T. O. 2017. Photocatalytic pathway toward degradation of environmental pharmaceutical pollutants: structure, kinetics and mechanism approach. *Catalysis Science & Technology* 7(20): 4548-4569.

de Moraes, N. P., Silva, F. N., da Silva, M. L. C. P., Campos, T. M. B., Thim, G. P., & Rodrigues, L. A. 2018. Methylene blue photodegradation employing hexagonal prism-shaped niobium oxide as heterogeneous catalyst: Effect of catalyst dosage, dye concentration, and radiation source. *Materials Chemistry and Physic* 214: 95-106.

Din, M. I. & Khalid, R. 2023. Photocatalysis of pharmaceuticals and organic dyes in the presence of silver-doped TiO_2 photocatalyst–A critical review. International *Journal of Environmental Analytical Chemistry* 1-25.

El Sharkawy, H. M., Shawky, A. M., Elshypany, R., & Selim, H. 2023. Efficient photocatalytic degradation of organic pollutants over TiO_2 nanoparticles modified with nitrogen and MoS_2 under visible light irradiation. *Scientific Reports* 13(1): 8845.

Hassan, N. S. & Jalil, A. A. 2022. A review on self-modification of zirconium dioxide nanocatalysts with enhanced visible-light-driven photodegradation of organic pollutants. *Journal of Hazardous Materials* 423: 126996.

Huang, C., & Peng, B. (2021). Photocatalytic degradation of patulin in apple juice based on nitrogen-doped chitosan-TiO_2 nanocomposite prepared by a new approach. *Lwt* 140: 110726.

Jallouli, S., Chouchene, K., Ben Hmida, M., & Ksibi, M. 2022. Application of sequential combination of electro-coagulation/electro-oxidation and adsorption for the treatment of hemodialysis wastewater for possible reuse. *Sustainability* 14(15): 9597.

Jana, D. K., Bhunia, P., Adhikary, S. D., & Bej, B. 2022. Optimization of effluents using artificial neural network and support vector regression in detergent industrial wastewater treatment. *Cleaner Chemical Engineering* 3: 100039.

Kasinathan, K., Marimuthu, K., Samayanan, S., & Yim, J. H. 2023. A biopolymer functionalized two-dimensional WS_2@ TiO_2 nanocomposite for in vitro biomedical and photocatalytic applications: facile synthesis and characterization. *Journal of Materials Chemistry B* 11(14): 3089-3096.

Kerkulah, E. N., Jin, G., Huang, J., Huang, X., Liu, Y., & Peng, H. 2023. A mini review on treatment of wastewater with membrane technology. *Journal of Basic & Applied Sciences* 19: 86-96.

Kumari, H., Sonia, Suman, Ranga, R., Chahal, S., Devi, S., Sharma, S., Kumar, S., Kumar, P., Kumar, S. & Kumar, A. 2023. A review on photocatalysis used for wastewater treatment: dye degradation. *Water, Air, & Soil Pollution* 234(6): 349.

Luo, M., Zhang, X., Long, T., Chen, S., Zhan, M., Zhu, X., & Yu, R. 2023. Modeling and optimization study on degradation of organic contaminants using nZVI activated persulfate based on response surface methodology and artificial neural network: a case study of benzene as the model pollutant. *Frontiers in Chemistry* 11: 1270730.

Madkhali, N., Prasad, C., Malkappa, K., Choi, H. Y., Govinda, V., Bahadur, I., & Abumousa, R. A. 2023. Recent update on photocatalytic degradation of pollutants in waste water using TiO_2-based heterostructured materials. *Results in Engineering* 17: 100920.

Majnis, M. F., Yee, O. C., Adnan, M. A. M., Hamid, M. R. Y., Shaari, K. Z. K., & Julkapli, N. M. 2022. Photoactive of Chitosan-ZrO_2/TiO_2 thin film in catalytic degradation of malachite green dyes by solar light. *Optical Materials* 124: 111967.

Manoharan, K., Srinivasaperumal, P., Murali, G., & Manjuvardhan, N. 2023. Dye Industries are a Threat to the Environment: An Assessment of Groundwater Characteristics. *Asian Journal of Water, Environment and Pollution* 20(3): 47-55.

Norman, M. A. M., Sivakumar, K., Ab Patar, M. N. A., & Mahmud, J. 2022. A Prediction Model for Natural Frequencies on Kevlar/Glass Hybrid Laminated Composite using Artificial Neural Networks (ANN). *International Journal of Integrated Engineering* 14(5): 207-214.

Rezai, B., & Allahkarami, E. 2021. Application of neural networks in wastewater degradation process for the prediction of removal efficiency of pollutants. *Soft Computing Techniques in Solid Waste and Wastewater Management*, Elsevier.

Saad, I., Ralha, N., Abukhadra, M. R., Al Zoubi, W., & Ko, Y. G. 2023. Recent advances in photocatalytic oxidation techniques for decontamination of water. *Journal of Water Process Engineering* 52: 103572.

Shahryari, Z., Sharifi, A., & Mohebbi, A. 2013. Artificial neural network (ANN) approach for modeling and formulation of phenol adsorption onto activated carbon. *Journal of Engineering Thermophysics* 22(4): 322-336.

Sheela, K. G., & Deepa, S. N. 2013. Review on methods to fix number of hidden neurons in neural networks. *Mathematical problems in engineering* 2013(1): 425740.

Taib, M. A. A., Mohd Adnan, M. A., Majnis, M. F., & Muhd Julkapli, N. 2023. *Photoactive Titanium Dioxide Nanoparticles Hybrid for Dye Removal Under Light Irradiation*. Singapore: Springer Nature Singapore.

Tian, J., Shao, Q., Zhao, J., Pan, D., Dong, M., Jia, C., Ding, T., Wu, T. & Guo, Z. 2019. Microwave solvothermal carboxymethyl chitosan templated synthesis of TiO_2/ZrO_2 composites toward enhanced photocatalytic degradation of Rhodamine B. *Journal of colloid and interface science* 541: 18-29.

Wang, H., Ren, Q., Xiao, L., Chen, L., He, Y., Yang, L., Sun, Y. & Dong, F. 2022. The spatially separated active sites for holes and electrons boost the radicals generation for toluene degradation. *Journal of Hazardous Materials* 437: 129329

Wu, Y., Guan, M., Chang, X., Wang, J., & Xu, S. 2023. Homogeneous double-layer TiO_2-ZrO_2-SiO_2 photocatalyst with multi-heterojunction structure for enhanced visible light-responsive photocatalytic activity. *Journal of Molecular Liquids* 369: 120959.

Zulfiqar, M., Samsudin, M. F. R., & Sufian, S. 2019. Modelling and optimization of photocatalytic degradation of phenol via TiO_2 nanoparticles: An insight into response surface methodology and artificial neural network. *Journal of Photochemistry and Photobiology A: Chemistry* 384: 112039.